OPEN

Tilted Microstrip Phased Arrays With Improved Electromagnetic Decoupling for Ultrahigh-Field Magnetic Resonance Imaging

Yong Pang, PhD, Bing Wu, PhD, Xiaohua Jiang, PhD, Daniel B. Vigneron, PhD, and Xiaoliang Zhang, PhD

Abstract: One of the technical challenges in designing a dedicated transceiver radio frequency (RF) array for MR imaging in humans at ultrahigh magnetic fields is how to effectively decouple the resonant elements of the array. In this work, we propose a new approach using tilted microstrip array elements for improving the decoupling performance and potentially parallel imaging capability.

To investigate and validate the proposed design technique, an 8-channel volume array with tilted straight-type microstrip elements was designed, capable for human imaging at the ultrahigh field of 7 Tesla. In this volume transceiver array, its electromagnetic decoupling behavior among resonant elements, RF field penetration to biological samples, and parallel imaging performance were studied through bench tests and in vivo MR imaging experiments.

In this specific tilted element array design, decoupling among array elements changes with the tilted angle of the elements and the best decoupling can be achieved at certain tilted angle. In vivo human knee MR images were acquired using the tilted volume array at 7 Tesla for method validation.

Results of this study demonstrated that the electromagnetic decoupling between array elements and the B1 field strength can be improved by using the tilted element method in microstrip RF coil array designs at the ultrahigh field of 7T.

(*Medicine* 93(28):e311)

Abbreviations: FDTD = finite-difference time-domain, FOV = field of view, g-factor = geometry factor, GRAPPA = generalized autocalibrating partially parallel acquisition, ID = inner diameter, MRI = magnetic resonance imaging, MTL = microstrip transmission line, NEX = number of excitation, OD = outer diameter, RF = radio frequency, SNR = signal-to-noise ratio, TE = echo time, TR = repetition time.

Editor: Michael Albert Thomas.
Received: August 19, 2014; revised: October 28, 2014; accepted: November 5, 2014.
From the Department of Radiology and Biomedical Imaging, University of California San Francisco, San Francisco, CA (YP, BW, DBV, XZ); Department of Electrical Engineering, Tsinghua University, Beijing, China (XJ); UC Berkeley/UCSF Joint Graduate Group in Bioengineering, San Francisco & Berkeley (DBV, XZ); and California Institute for Quantitative Biosciences (QB3), San Francisco, CA (DBV, XZ).
Correspondence: Xiaoliang Zhang, Department of Radiology and Biomedical Imaging, University of California San Francisco, San Francisco, CA (e-mail: zhanglabuc@gmail.com).
National Natural Science Foundation of China Grant (51228702), NIH grants R01EB008699, P41EB013598, and K99EB015487, and a Springer Med Fund Award.
The authors have no conflicts of interest to disclose.
Yong Pang and Bing Wu contributed equally to this work.

ISSN: 0025-7974
DOI: 10.1097/MD.0000000000000311

INTRODUCTION

Magnetic resonance imaging (MRI) has become one of the most important non-invasive imaging modalities used in clinical medicine.[1–3] The fact that signal to noise ratio (SNR) is proportional to the static magnetic field strength[4] has resulted in the rapid development of high and ultrahigh field MRI such as 3T, 7T, and beyond.[5–12] With the increase of the Larmor frequency at high fields, radiation losses and interaction between RF coil and imaging subject increase, leading to degraded quality factors, and MR signal intensity. These problems become more pronounced at ultrahigh magnetic fields such as 7T where the proton Larmor frequency reaches the high frequency of 300-MHz range. Therefore, there is a demand for designing sensitive high-frequency radio frequency (RF) coils for efficient MR signal excitation and detection at high and ultrahigh magnetic fields.[13,14]

The RF coil array was firstly introduced to MR signal acquisition to improve SNR[15] for large field-of-view (FOV) imaging. In recent years, this technique has been utilized in parallel acquisition[16–22] and parallel transmission[23–25] to accelerate imaging speed. Transmit/receive (or transceiver) coil arrays are also essential for RF excitation field (referred to as B_1+) shimming by using independent phase and amplitude control of each array element[26–30] to address field inhomogeneity problems in high dielectric and conductive biological samples, such as the human body at ultrahigh fields.[28,31–35] These techniques require dedicated transceiver arrays with sufficient electromagnetic decoupling among the array elements. However, due to the significantly increased coupling among resonant elements of an array at ultrahigh magnetic fields,[34,36–39] it is technically challenging to implement such a dedicated transceiver array. Conventional decoupling methods such as the use of low impedance preamplifier,[15] which are usually used in receive-only arrays, are not readily feasible for transceiver array designs. Dedicated decoupling circuits, either capacitive or inductive, have been applied to decouple an n-element array using a 2n-port decoupling interface.[40] This method may become complicated and increase electric losses, especially for a massive number of coil elements in an array.

To reduce radiation losses and increase the RF coil efficiency, the microstrip transmission line (MTL)[41,42] approach has been introduced for RF coil design at ultrahigh fields.[10–14,34,43] Microstrip coils can readily be operated at ultrahigh Larmor frequencies such as 298 MHz (7 Tesla)[10,12] and 400 MHz (9.4 Tesla)[13,14,43] for commonly desired coil size. Its simple structure and high frequency operation capability make coil design and construction convenient, especially for

ultrahigh field volume coils[12,44] and coil arrays[34–36,39,45,46] with complicated mechanical structures. Due to the inherent decoupling among microstrip resonators, microstrip transceiver arrays have demonstrated excellent decoupling performance and have been realized at ultrahigh field MRI.[34,35,45,47–49] However, for RF coil arrays with a massive number of elements, due to the reduced distance between coil elements where the microstrip decoupling conditions are often unable to be met, achieving better than −18 dB decoupling between resonant elements is technically challenging in practice.

In this work, an improved decoupling method for microstrip transceiver array designs based on tilted element technique[50–52] was proposed and investigated. A specific microstrip transceiver array with 1.3 cm thick Teflon substrate, 1.3 cm wide microstrip resonator and 16 cm length, operating at 300 MHz, was designed and constructed for this investigation at the ultrahigh field of 7T. Bench tests on a network analyzer were made to measure the B_1 strength variation with the tilted angle, and compare the mutual coupling between a tilted array and non-tilted array. Numerical simulation by using Finite-Difference Time-Domain (FDTD) method was used to compare the B_1 field distribution between 2 microstrip resonators with 0° and 30° (optimized for decoupling) tilted angles. In vivo MR images were acquired using the transceiver array from healthy human volunteers. To investigate parallel imaging performance of the proposed tilted arrays, GRAPPA accelerated parallel imaging[18] was used for image reconstruction at various acceleration rates. The geometry factor (g-factor)[17] for 1D accelerated imaging were also calculated and evaluated.

METHODS

Design of Coil Array With Titled Straight-Type Microstrip Elements

An 8-channel transceiver volume array with tilted straight-type microstrip elements was built. Each element was a capacitive terminated half-wavelength (λ/2) microstrip resonator with 1.3 cm width and 16 cm length as shown in Figure 1B. Termination capacitors were DLC2R7 (Dalian Dalicap Co., Ltd., Dalian, China) with a nominal capacitance of 2.7 pF and a variable capacitor (NMAP25HV, Voltronics Co., Salisbury, MD) ranging from 1 to 25 pF. The strip conductor was built on the surface of a Teflon substrate with 1.3 cm thickness and permittivity of 2.1. On the bottom of the substrate, there was a piece of adhesive copper tape acting as the ground plane. The resonant frequency of such a capacitive terminated λ/2 resonator can be estimated by solving the following equation[12]:

$$f_{re} = \frac{(2\pi f_{re} Z_0)^2 C_{t1} C_{t2} - 1}{2\pi Z_0 (C_{t1} + C_{t2})} \tan\left(\frac{2\pi l \sqrt{\varepsilon_{eff}}}{c} f_{re}\right) \quad (1)$$

where C_{t1} and C_{t2} are the capacitance of the termination capacitors of the microstrip resonator shown in Figure 1B. Z_0 is the characteristic impedance of the microstrip resonator. l and c denote the length of the microstrip conductor and the velocity of light in free space, respectively. ε_{eff} is the effective permittivity of the microstrip resonator.

A total of 8 elements were built on a supporting frame with 21 cm ID and 28 cm OD and the prototype of this volume array is shown in Figure 2. Thus each element can be tilted to any angle to become a tilted microstrip array. The cross section views of this tilted array and a regular array are shown in Figure 3. The tilted angle θ was defined tangentially to a circle crossing all coil elements as shown in Figure 3B. This structure also facilitated comparison between regular array and tilted array with different tilted angle. The impedance matching of each element was achieved by varying the trimmer capacitor (NMAP25HV, Voltronics Co.), which was connected in series to feed port of the microstrip resonator.

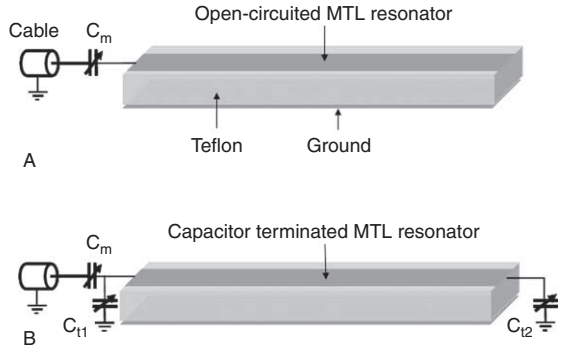

FIGURE 1. Diagrams of (A) typical open-circuited MTL resonator, (B) capacitor terminated MTL resonator.

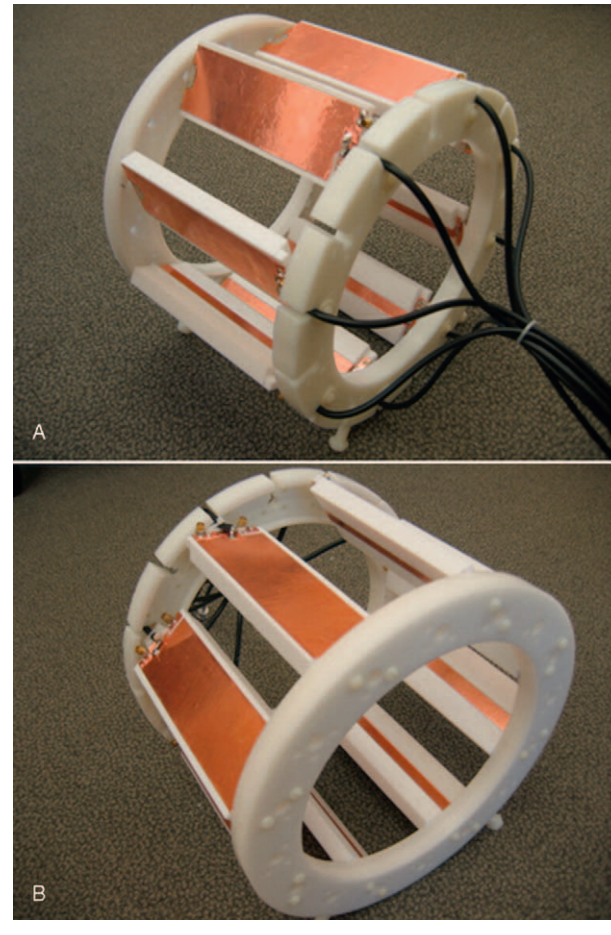

FIGURE 2. Prototype of the 8-channel transceiver volume array with tilted straight-type microstrip elements: views from left side (A) and right side (B).

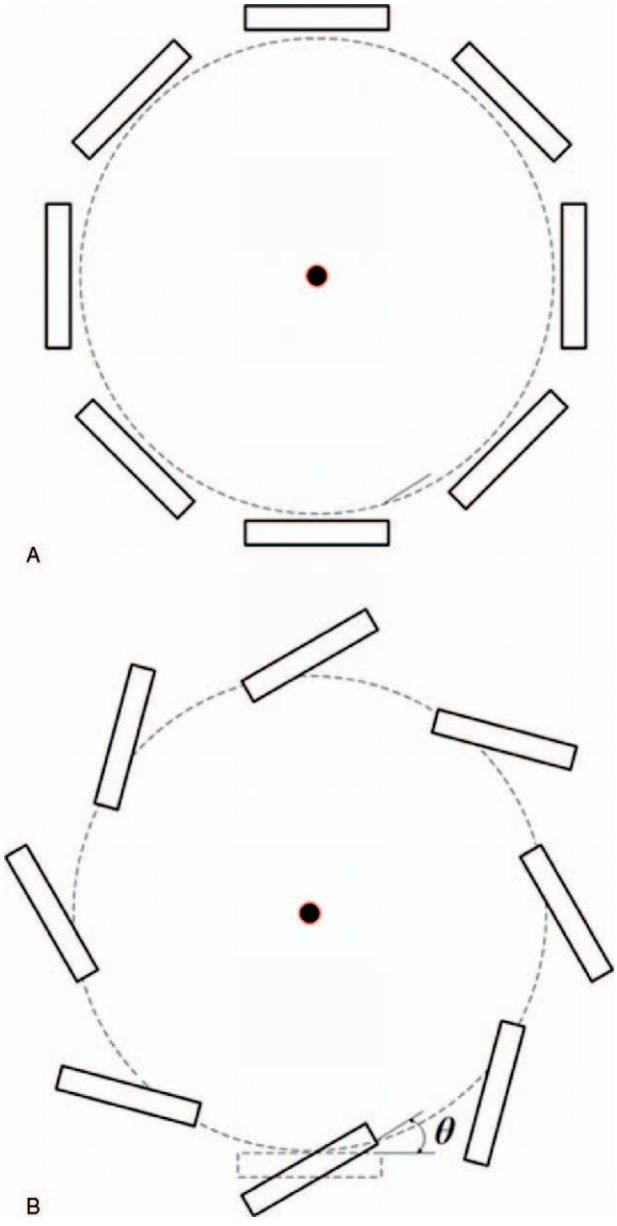

FIGURE 3. The cross-sectional view of a regular volume array (A) and the volume array with tilted elements (B). All the elements are tilted at an angle θ, which is indicated in (B). The center of the element will always keep on the circle at any tilt angle.

Bench Measurement and MR Test

MR imaging study with healthy human subjects on 7T MRI was obtained from the Committee on Human Research (CHR) at the University of California San Francisco (ie, UCSF's IRB). Subjects were provided informed written consent prior to participating in the study.

Bench test of the microstrip volume array with different tilted angle θ was made on an Agilent E5070B network analyzer. The transmission parameter S_{21} was used to measure the decoupling performance between the adjacent elements of the array. The decoupling performance, which varies with the tilted angle θ, then can be plotted as a function of θ. The mutual coupling between each pair of the elements in the coil array was also measured using the network analyzer, and the mutual coupling matrix was generated to show the decoupling performance of the array. MR imaging experiments with the tilted microstrip array was performed on a General Electric (GE) 7 Tesla whole body MR scanner. This scanner is equipped with 2 quadrature transmit channels and 2 T/R switchers. To test the transceiver arrays on this scanner, scan series were conducted by connecting 2 coil elements into the transmit channels each time, and combining all sub-images offline. Axial plane images of the human knee from a healthy volunteer were acquired with this array by using gradient echo sequences. The acquisition parameters used were TE = 7 ms, TR = 100 ms, matrix size = 256 × 256, receiver bandwidth = 15.6 kHz, field of view (FOV) = 14 cm, slice thickness = 3 mm, number of excitation (NEX) = 1.

Evaluation of Parallel Imaging Performance

To demonstrate the performance of the tilted array in parallel accelerated imaging, GRAPPA accelerated imaging was used for human knee image reconstruction. The acceleration was applied to phase encoding direction (y-axis) and 32 Auto-Calibration Signal (ACS) lines were acquired in the central region of the k-space to estimate the missing lines. GRAPPA reconstructions with acceleration factor from 2 to 8 were performed and were compared with the reference image reconstructed from the sum of squares method from full k-space data.

In addition, the noise correlation matrix was calculated to demonstrate the noise correlation among array elements. The spatial varying geometry factors (g-factors) were calculated using[17]:

$$g_\rho = \sqrt{[(S^H \Psi^{-1} S)^{-1}]_{\rho,\rho} (S^H \Psi^{-1} S)_{\rho,\rho}} \quad (2)$$

where ρ denote the index of voxel in the field of view, and S is the reduced Fourier encoding. ψ is the noise correlation matrix between channels. G-factor strongly depends on the voxel position and has a direct impact on SNR[17]:

$$\mathrm{SNR}_\rho^{\mathrm{red}} = \frac{\mathrm{SNR}_\rho^{\mathrm{full}}}{g_\rho \sqrt{R}} \quad (3)$$

where R is the reduction factor (or acceleration factor). This relationship means the SNR of the accelerated image is inversely proportional to the g-factor. The larger the g-factor, the worse the parallel imaging performance is. The average and maximum g-factors were plotted in term of acceleration factor to demonstrate the performance of the tilted array for accelerated parallel imaging.

RESULTS

Bench Measurements of Tilted Array With Straight-Type Microstrip Elements

Bench measurements of the tilted volume array with straight-type microstrip elements at different tilted angle θ from 0° to 40° are plotted in Figure 4. When $\theta = 0°$ this array is actually a regular microstrip array. It is shown that with the variation of the tilted angle, the decoupling between array elements changes obviously. For this specific microstrip array, the tilted angle of ~30° can be regarded as an inflexion point and at this tilted angle the decoupling between elements reaches

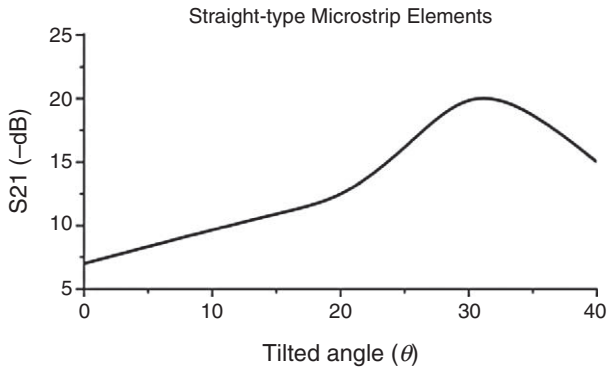

FIGURE 4. Decoupling between array elements of the volume transceiver array with tilted straight-type microstrip resonators measured in unloaded case. The black curve describes the transmission parameter S_{21} measurement varies with the tilted angle: between 0° and 30° the decoupling increases with the tilted angle, indicating that the self-cancellation from the ground plane can be compensated by tilting the elements.

optimal value of −22 dB. Compared with regular microstrip volume array with the same structure, the decoupling can be greatly improved without using any extra decoupling techniques.

To compare the isolation between each pair of elements in the tilted and non-tilted arrays, the mutual coupling matrices of the coil arrays with 0° to 30° tilted angles were measured and are shown in Figure 5. The tilted array achieved better than −20 dB mutual coupling while the conventional non-tilted array achieved better than −12 dB mutual coupling, demonstrating an improvement of at least 8 dB in decoupling performance by using the tilted element strategy.

From the bench test, it is also observed that the B_1 field was strengthened at the central region of the coil array when increasing the tilted angle in the range of 0° to 90°. As shown in Figure 6, the B_1 field strength was increased by 28% when the tilted angle was changed from 0° to 30°. Simulation comparison between 2 elements with 0° to 30° tilted angles in Figure 7 illustrates the change of the B_1+ field distribution in a human brain imaging area. With element tilting, the imaging coverage of coil elements is enlarged compared with that of non-tilted elements.

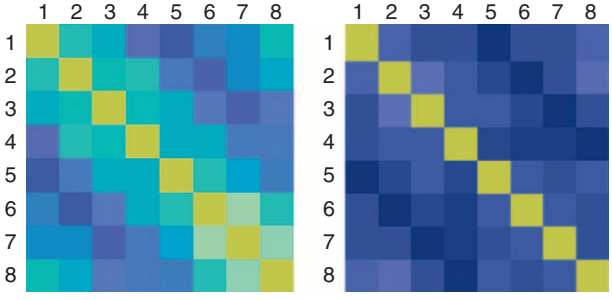

FIGURE 5. Mutual coupling matrices among all the coil elements of the microstrip array with 0° angle (left) and optimized 30° angle (right). The array with 0° angle can achieve better than −12 dB mutual coupling, while the array with 30° tilted angle can achieve better than −20 dB mutual coupling.

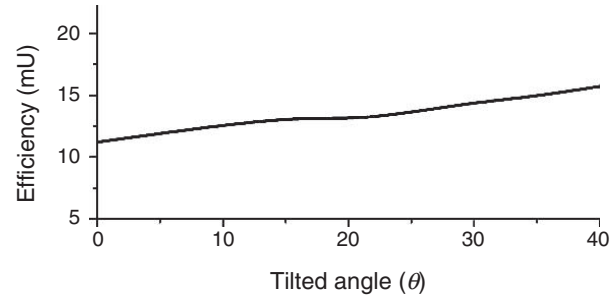

FIGURE 6. B_1 field strength of the microstrip array increases with tilted angle from 0° to 40°. The field strength is improved by approximately 28% at 30° tilted angle which is the optimized angle for achieving best decoupling for this specific MTL coil array design: Teflon substrate with 1.3 cm thickness, microstrip resonator with 1.3 cm width and 16 cm length.

Parallel Imaging Performance

Figure 8 shows the reconstructed images from in vivo human knee MR imaging. The first image is the reference image, which was reconstructed from full *k*-space data using a sum of squares method. The images from the second to the eighth were reconstructed using GRAPPA accelerated imaging method at acceleration factors of 2 to 8. It is clearly shown that with the increase of acceleration factor, the imaging speed was enhanced while SNR decreased. When the acceleration factor was smaller than 4, there was no obvious distortion to the image and the image quality was acceptable. For higher acceleration factor up to 8, obvious distortion can be observed in the reconstructed image. Tradeoffs must be made between the imaging speed and the SNR in parallel imaging. In Figure 9, the average and maximum g-factor is plotted as a function of acceleration factor, which demonstrates the parallel imaging performance at different acceleration factors.

CONCLUSIONS

In this study, a transceiver array design technique using tilted elements was investigated for microstrip coils numerically and experimentally. By using the tilted element strategy, mutual inductance between the coil elements could be diminished and thus element-decoupling performance of microstrip coil array could be improved. Bench test measurement was performed to compare the microstrip array with tilted elements and non-tilted elements in terms of RF field strength and the mutual coupling between each pair of elements, demonstrating an improvement

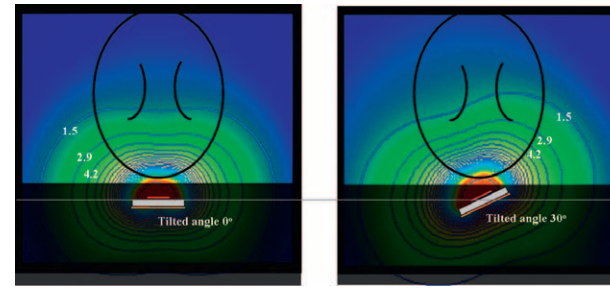

FIGURE 7. Simulation result of the RF field penetration of an MTL resonator with 0° (left) and 30° (right) tilt angles. The tilted resonator shows larger image coverage within the imaging object. The RF field strength is measured in mGauss.

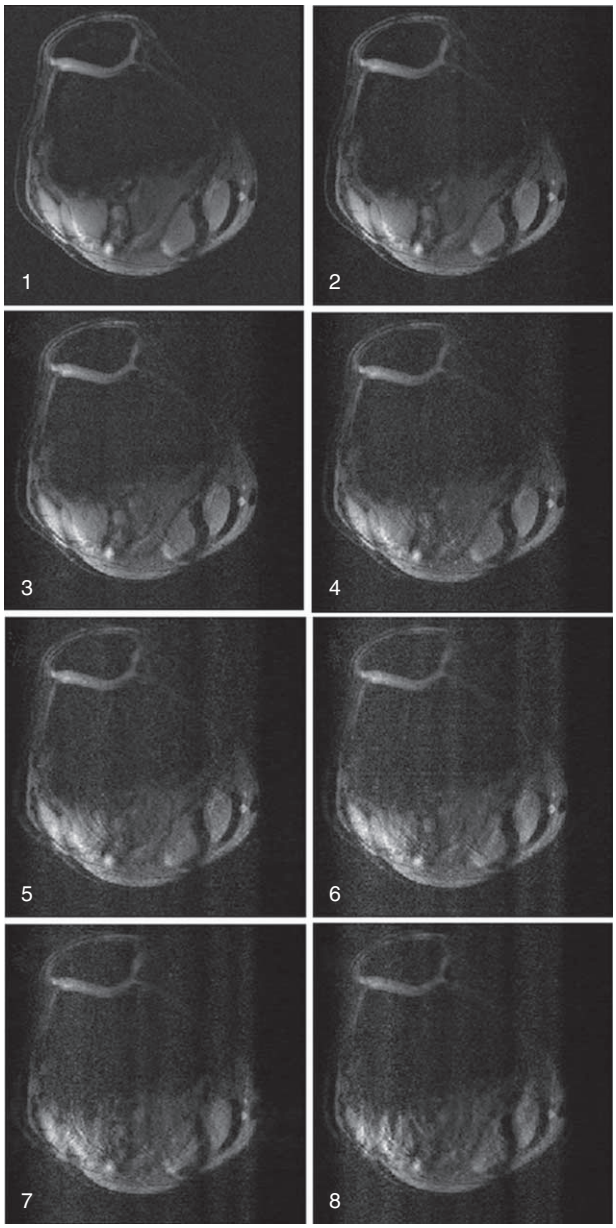

FIGURE 8. GRAPPA reconstructed human knee images acquired using the volume array with tilted microstrip elements. The imaging matrix size is 256 by 256. In the acquisition, 32 ACS lines were used for estimating the missing *k*-space lines. Number of excitation = 1. Image 1 is a reference image reconstructed from full sampled *k*-space using sum-of-squares method. Images 2 to 8 are the results of accelerated imaging at acceleration factors of 2 to 8. As expected, the image quality degrades with the increase of the imaging speed when using parallel imaging.

in the RF field penetration and the decoupling performance of the proposed tilted element array. Numerical simulations using FDTD method were also conducted to compare the B_1+ field distribution in the 2 different cases (ie, tilted and non-tilted), showing that the tilted array could obtain larger imaging coverage for this specific design. It might be interesting to investigate the tilted element method for microstrip arrays with a large number of array elements, where the decoupling conditions are often unable to be satisfied due to the reduced distance between array elements, resulting in insufficient decoupling for imaging acquisitions with reasonable quality.

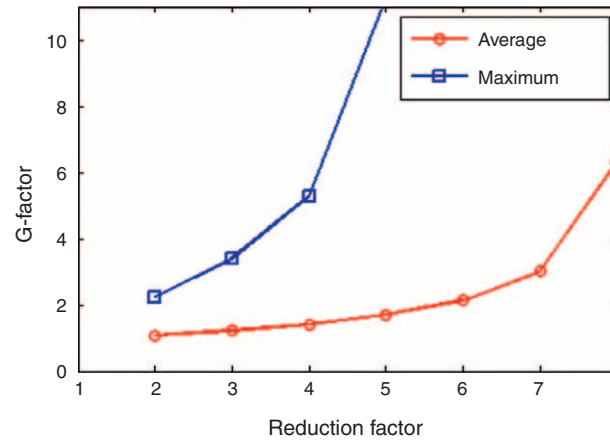

FIGURE 9. Average and maximum g-factors are plotted as function of acceleration factor. The average g-factor is 1.08, 1.21, and 1.41 at acceleration factors of 2, 3, and 4, demonstrating reasonably good performance for accelerated parallel imaging.

REFERENCES

1. Riederer SJ. MR imaging: its development and the recent Nobel Prize. *Radiology.* 2004;231:628–631.
2. Lauterbur PC. Image formation by induced local interactions: examples employing nuclear magnetic resonance. *Nature.* 1973;242:190–191.
3. Mansfield P. Multi-planar image formation using NMR spin echoes. *J Phys Chem.* 1977;10:L55.
4. Hoult DI, Richards RE. The signal-to-noise ratio of the nuclear magnetic resonance experiment. *J Magn Reson.* 1976;24:171–185.
5. Ugurbil K, Garwood M, Ellermann J, et al. Imaging at high magnetic fields: initial experiences at 4T. *Magn Reson Q.* 1993;9:259–277.
6. Ugurbil K, Hu X, Chen W, et al. Functional mapping in the human brain using high magnetic fields. *Philos Trans R Soc Lond B Biol Sci.* 1999;354:1195–1213.
7. Wada H, Sekino M, Ohsaki H, et al. Prospect of high-field MRI. *IEEE Trans Appl Sperconductivity.* 2010;20:115–122.
8. Vaughan JT, Garwood M, Collins CM, et al. 7T vs. 4T: RF power, homogeneity, and signal-to-noise comparison in head images. *Magn Reson Med.* 2001;46:24–30.
9. Abduljalil AM, Kangarlu A, Zhang X, et al. Acquisition of human multislice MR images at 8 Tesla. *J Comput Assist Tomogr.* 1999;23:335–340.
10. Zhang X, Ugurbil K, Chen W. Microstrip RF surface coil design for extremely high-field MRI and spectroscopy. *Magn Reson Med.* 2001;46:443–450.
11. Yacoub E, Shmuel A, Pfeuffer J, et al. Imaging brain function in humans at 7 Tesla. *Magn Reson Med.* 2001;45:588–594.
12. Zhang X, Ugurbil K, Sainati R, et al. An inverted-microstrip resonator for human head proton MR imaging at 7 Tesla. *IEEE Trans Biomed Eng.* 2005;52:495–504.
13. Vaughan JT. An improved volume coil for high field MRI. In: *Proceedings of ISMRM Annual Scientific Meeting*, Philadelphia, PA. 1999:p. 167.

14. Vaughan JT. RF coil for imaging system US Patent 6,633,161 2003.
15. Roemer PB, Edelstein WA, Hayes CE, et al. The NMR phased array. *Magn Reson Med.* 1990;16:192–225.
16. Sodickson DK, Manning WJ. Simultaneous acquisition of spatial harmonics (SMASH): fast imaging with radiofrequency coil arrays. *Magn Reson Med.* 1997;38:591–603.
17. Pruessmann KP, Weiger M, Scheidegger MB, et al. SENSE: sensitivity encoding for fast MRI. *Magn Reson Med.* 1999;42:952–962.
18. Griswold MA, Jakob PM, Heidemann RM, et al. Generalized autocalibrating partially parallel acquisitions (GRAPPA). *Magn Reson Med.* 2002;47:1202–1210.
19. Griswold MA, Jakob PM, Nittka M, et al. Partially parallel imaging with localized sensitivities (PILS). *Magn Reson Med.* 2000;44:602–609.
20. Heidemann RM, Griswold MA, Haase A, et al. VD-AUTO-SMASH imaging. *Magn Reson Med.* 2001;45:1066–1074.
21. Lin FH, Kwong KK, Belliveau JW, et al. Parallel imaging reconstruction using automatic regularization. *Magn Reson Med.* 2004;51:559–567.
22. Ji JX, Son JB, Rane SD. PULSAR: a matlab toolbox for parallel magnetic resonance imaging using array coils and multiple channel receivers. *Concepts Magn Reson B: Magn Reson Eng.* 2007;31B:24–36.
23. Katscher U, Bornert P, Leussler C, et al. Transmit SENSE. *Magn Reson Med.* 2003;49:144–150.
24. Zhu Y. Parallel excitation with an array of transmit coils. *Magn Reson Med.* 2004;51:775–784.
25. Grissom W, Yip CY, Zhang Z, et al. Spatial domain method for the design of RF pulses in multicoil parallel excitation. *Magn Reson Med.* 2006;56:620–629.
26. Vaughan JT, Adriany G, Snyder CJ, et al. Efficient high-frequency body coil for high-field MRI. *Magn Reson Med.* 2004;52:851–859.
27. Boskamp EB, Lee RF. Whole body LPSA transceive array with optimized transmit homogeneity. p. 903.
28. Metzger GJ, Snyder C, Akgun C, et al. Local B1+ shimming for prostate imaging with transceiver arrays at 7T based on subject-dependent transmit phase measurements. *Magn Reson Med.* 2008;59:396–409.
29. Zhang X, Pang Y. Parallel excitation in ultrahigh field human mr imaging and multi-channel transmit system. *OMICS J Radiol.* 2012;1:doi:10. 4172/2167-79641000e110.
30. Pang Y, Yu B, Zhang X. Hepatic fat assessment using advanced magnetic resonance imaging. *Quant Imaging Med Surg.* 2012;2:213–218.
31. Sekino M, Kim D, Ohsaki H. Finite-difference time-domain simulations of radio frequency electromagnetic fields and signal inhomogeneities in ultrahigh-field magnetic resonance imaging systems. *J Appl Phys.* 2008;103:07A318.
32. Yang QX, Wang J, Zhang X, et al. Analysis of wave behavior in lossy dielectric samples at high field. *Magn Reson Med.* 2002;47:982–989.
33. Yang QX, Mao W, Wang J, et al. Manipulation of image intensity distribution at 7.0T: passive RF shimming and focusing with dielectric materials. *J Magn Reson Imaging.* 2006;24:197–202.
34. Adriany G, Van de Moortele PF, Wiesinger F, et al. Transmit and receive transmission line arrays for 7 Tesla parallel imaging. *Magn Reson Med.* 2005;53:434–445.
35. Adriany G, Van de Moortele PF, Ritter J, et al. A geometrically adjustable 16-channel transmit/receive transmission line array for improved RF efficiency and parallel imaging performance at 7 Tesla. *Magn Reson Med.* 2008;59:590–597.
36. Zhang X, Burr AR. Zhu X et al. A dual-tuned microstrip volume coil array for human head parallel 1H/31P MRI/MRS at 7T. In: *Proceedings of ISMRM Annual Scientific Meeting*, Miami Beach, FL. 2005:p. 896.
37. Wiggins GC, Triantafyllou C, Potthast A, et al. 32-channel 3 Tesla receive-only phased-array head coil with soccer-ball element geometry. *Magn Reson Med.* 2006;56:216–223.
38. Li Y, Xie Z, Pang Y, et al. ICE decoupling technique for RF coil array designs. *Med Phys.* 2011;38:4086–4093.
39. Wu B, Zhang X, Wang C, et al. Flexible transceiver array for ultrahigh field human MR imaging. *Magn Reson Med.* 2012;68:1332–1338.
40. Lee RF, Giaquinto RO, Hardy CJ. Coupling and decoupling theory and its application to the MRI phased array. *Magn Reson Med.* 2002;48:203–213.
41. Cohn SB. Shielded coupled-strip transmission line. *IRE Trans.* 1955;MTT-3:29–38.
42. Wheeler H. Transmission-line properties of a strip on a dielectric sheet on a plane. *IEEE Trans Microwave Theory Tech.* 1977;25:631–647.
43. Zhang X, Zhu XH, Chen W. Higher-order harmonic transmission-line RF coil design for MR applications. *Magn Reson Med.* 2005;53:1234–1239.
44. Zhang X, Ugurbil K, Chen W. A microstrip transmission line volume coil for human head MR imaging at 4T. *J Magn Reson.* 2003;161:242–251.
45. Wu B, Wang C, Kelley DA, et al. Shielded microstrip array for 7T human MR imaging. *IEEE Trans Med Imaging.* 2010;29:179–184.
46. Wu B, Wang C, Lu J, et al. Multi-channel microstrip transceiver arrays using harmonics for high field MR imaging in humans. *IEEE Trans Med Imaging.* 2012;31:183–191.
47. Wu B, Zhang X, Qu P, et al. Capacitively decoupled tunable loop microstrip (TLM) array at 7T. *Magn Reson Imaging.* 2007;25:418–424.
48. Wu B, Zhang X, Qu P, et al. Design of an inductively decoupled microstrip array at 9.4T. *J Magn Reson.* 2006;182:126–132.
49. Wu B, Wang C, Krug R, et al. 7T human spine imaging arrays with adjustable inductive decoupling. *IEEE Trans Biomed Eng.* 2010;57:397–403.
50. Hardy CJ, Pelc JS, Zhu Y, et al. Low coupling with low g factor using venetian-blind arrays. p. 677.
51. Pang Y, Wu B, Zhang X. Reduce power deposition using microstrip array with tilted elements at 7T. In: *Proceedings of ISMRM Annual Scientific Meeting*, Toronto, Ontario. 2008:p. 47.
52. Wu B, Pang Y, Wang C, et al. Tilted transceiver array for ultra-high field MRI. In: *Proceedings of ISMRM Annual Scientific Meeting*, Toronto, Ontario. 2008:p. 3825.